



A Comparative Study of the Atomic-Layer-Deposited Tungsten Thin Films as Nucleation Layers for W-Plug Deposition

Soo-Hyun Kim,^{a,*} Nohjung Kwak,^a Jinwoong Kim,^a and Hyunchul Sohn^{b,z}

^aHynix Semiconductor, Incorporated, Research and Development Division, Ami-ri, Bubal-eub, Icheon-si, Kyoungki-do 467-701, Korea

^bDepartment of Ceramic Engineering, Yonsei University, Seodaemun-gu, Seoul 120-749, Korea

The properties of three different kinds of atomic-layer-deposited (ALD) W thin films were comparatively characterized and investigated as nucleation layers for the W-plug process of 70 nm design-rule dynamic random access memory. ALD-W (A) film was deposited using alternating exposures of WF_6 and SiH_4 and ALD-W (B) film was treated with B_2H_6 for 5 s prior to W ALD using WF_6 and SiH_4 . Finally, ALD-W (C) film was deposited using alternating exposures of WF_6 and B_2H_6 . All the ALD-W films showed excellent step coverage at the contact with an aspect ratio of ~ 14 , but their resistivities were as high as 125–145 $\mu\Omega$ cm at the thickness of 20 nm. High resistivities of ALD-W films are discussed on the basis of impurities cooperation such as Si and B, phase (body-centered-cubic α -W or primitive cubic β -W), crystallinity (crystalline or amorphous), and grain size. It was found that ALD-W (C) film formed an amorphous phase, which was stable until 900°C annealing. This is clearly different from ALD-W (A) and ALD-W (B) with polycrystalline grains of α -W and β -W, and β -W was transformed to α -W after 800°C annealing. The formation of amorphous W resulted in the formation of large-size grains of chemical-vapor-deposited W film deposited on ALD-W (C) and the reduction in the resistivity of W-plug stack. The integration results showed that the reduced resistivity of W-plug stack with ALD-W (C) provided a significantly lower resistance at the W bit line contact. Another advantage of the integration scheme with ALD-W (C) was its stable contact resistance at the ultrahigh aspect ratio (UHAR) contact even though the step coverage of the underlayer, TiN, was poor. It was also found that the B_2H_6 pretreatment was effective for obtaining the low and stable contact resistance at UHAR contact.

© 2006 The Electrochemical Society. [DOI: 10.1149/1.2222966] All rights reserved.

Manuscript submitted March 20, 2006; revised manuscript received May 22, 2006. Available electronically July 26, 2006.

Atomic layer deposition (ALD) is one of the most promising technologies related to preparing thin films for future generation microelectronic device fabrication.^{1,2} Several key features of ALD include the capability of depositing ultrathin, highly uniform, and high-purity film with near 100% step coverage in a complicated geometry. This is desirable for the ever-shrinking device. ALD is mainly applied in semiconductor devices, including Cu diffusion barrier, high-permittivity (high- k) gate or capacitor dielectrics, and metal gate or capacitor electrodes as well. One of the attractive features about using ALD in microelectronic devices, which is the main subject of this paper, is the nucleation layer deposition for W-plug process at ultrahigh aspect ratio (UHAR) contact of advanced dynamic random access memory (DRAM) with a stacked capacitor. The recent *International Technology Roadmap for Semiconductors*³ shows that a 16:1 aspect ratio (AR) contact needs to be filled at 70 nm technology node DRAM contact and with 17:1 at 50 nm. Though a chemical-vapor-deposited (CVD) W film, generally deposited by the reaction of WF_6 and SiH_4 , has been successfully used as a nucleation layer,⁴ its limited conformality at UHAR contact can induce potential problems such as the seam or void in final W-plug, leading to the degradation in contact resistance.^{5,6} In this respect, the ALD-W process is expected to solve any potential problems in connection with preparing ultrathin and conformal nucleation layer for W-plug process.

W ALD is the most successful case among elemental metal ALD processes. This is mainly due to the fact that W ALD is accomplished from the well-known good metal-containing precursor, WF_6 , and good reducing agents, silane or borane compound. The successful deposition of ALD-W was first reported by Klaus et al.⁷ They used a sequential supply of WF_6 and disilane (Si_2H_6) at the temperature of lower than 325°C, which is low enough for semiconductor device fabrication. Later, it was reported that the ALD-W films could be deposited by using diborane (B_2H_6) as a reducing agent of WF_6 at 300°C.⁸ The ALD-W process using a very similar reducing agent to disilane, silane (SiH_4), was also extensively investigated.⁹⁻¹¹ Recently, the effect of B_2H_6 pretreatment on ALD-W film deposited using an alternating supply of WF_6 and SiH_4 was

reported.¹¹ The results showed that the B_2H_6 pretreatment could enhance the nucleation of ALD-W on SiO_2 and also enhance the step coverage of ALD-W films at UHAR contact.

While there has been much effort in developing ALD-W processes, there have been very limited investigations on the electrical properties at the UHAR contact of semiconductor devices. Thus, it is still not easy to compare the electrical performances when the various ALD-W films are integrated to the semiconductor device. To evaluate the comparative performance of each of these films, therefore, it is necessary to test the same thickness of the film at the contact with the same dimension. It is also critical to understand the key film properties to affect the electrical performances at the UHAR contact.

In this study, the properties of three kinds of ALD-W films were comparatively characterized and tested as nucleation layers for W-plug process of 70 nm design-rule DRAM. The systematic investigations on the film properties such as resistivity, composition, impurities, phase, and microstructure were carried out. In addition, the properties of CVD-W films deposited on different ALD-W films were also characterized. We found that the properties of CVD-W films were much affected by the ALD-W nucleation layers, which in turn has some effect on the electrical performance of each W-plug scheme. As the potential applications of ALD-W films in microelectronics also include the metal gate electrode, capacitor electrode for memory device, or diffusion barrier for Cu metallization, further studies need to be performed but are not discussed herein.

Experimental

CVD-TiN film deposited using the reaction of $TiCl_4$ and NH_3 at 580°C or periodically plasma-treated metallorganic CVD (MOCVD)-TiN film deposited at 450°C using tetrakis-dimethyl-amido-titanium $\{Ti[N(CH_3)_2]_4, TDMAT\}$ as a precursor were used as substrates for W growth. The properties of ALD-W films to be investigated in this study were almost same. Slight differences with TiN films were observed in their roughness and texture, which are generally dependent on the underlayer. Three different ALD W films were prepared as nucleation layers for W-plug deposition using commercial 200 mm chambers. Among them, two ALD-W films [ALD-W (A) and ALD-W (B)] were deposited using a sequential supply of WF_6 and SiH_4 as reactants and one ALD-W film [ALD-W

* Electrochemical Society Active Member.

^z E-mail: hyunchul.sohn@yonsei.ac.kr

(C)] using WF_6 and B_2H_6 . The ALD-W (B) was pretreated with 200 sccm of B_2H_6 for 5 s before ALD.¹¹ The deposition temperature for ALD-W films was 300°C.

The thicknesses of ALD-W films were determined from the cross-sectional view transmission electron microscopy (XTEM) analysis. The film properties were analyzed with various tools and compared with each other; sheet resistance by 4-point probe, surface roughness by atomic force microscopy (AFM), composition and impurities content by X-ray photoelectron spectroscopy (XPS) or Auger electron spectroscopy (AES) and secondary ion mass spectrometry (SIMS), film crystallinity and phase by X-ray diffractometry (XRD), and microstructure and phase by plan-view and cross-sectional view TEM. The step coverage of ALD-W films were investigated at the contact hole (height $\sim 3.52 \mu\text{m}$ and aspect ratio ~ 15). Aspect ratio of the contact was determined by dividing the contact height with its diameter at the top of the contact. Finally, the thermal stability and phase transformation behavior were investigated by sheet resistance measurement and XRD after high-temperature annealing. The annealing was performed for 30 min at the processing pressure of 5×10^{-5} Torr. In order to understand the effect of ALD-W layers on the properties of CVD-W films growing on them, CVD-W films deposited by H_2 reduction of WF_6 at $\sim 390^\circ\text{C}$ were deposited in situ after ALD-W depositions. Their properties were also analyzed by 4-point probe, AFM, AES, and plan-view scanning electron microscopy (SEM).

In order to study the electrical properties when the ALD-W film was used as a nucleation layer for W-plug process, Si wafers were processed through a 70 nm design-rule DRAM process flow. Prior to ALD-W depositions, TiN films (TiCl_4 -based CVD-TiN and periodically plasma-treated MOCVD-TiN) were deposited as glue/barrier layers. Then, ALD-W films were deposited and following this, W-plug processes were performed in situ. Blanket W deposition and etch-back were used to fill the contacts followed by metal line deposition. Finally, metal line patterning was accomplished. The contact resistance was measured using a contact chain structure connecting the W bit line and metal line with two different contact sizes and aspect ratios.

Results and Discussion

Properties of ALD-W films.— All the ALD-W films showed excellent step coverage irrespective of B_2H_6 pretreatment and reducing agents of WF_6 at UHAR contact holes (AR ~ 15) as shown by the XTEM images in Fig. 1. Here, prior to ALD-W depositions, TiCl_4 -based CVD-TiN films were deposited as barrier layers. The excellent step coverage of the nucleation layers ensured excellent filling of W-plug. However, the B_2H_6 pretreatment enhanced the step coverage of ALD-W film deposited using WF_6 and SiH_4 , especially when the step coverage of underlayer TiN was very poor.¹¹

Resistivity of metal film is an important consideration because it represents the overall films properties. Figure 2 shows the resistivities of ALD-W films as a function of film thickness. All the ALD-W films showed high resistivities of 125–145 $\mu\Omega \text{ cm}$ at the thickness of $\sim 20 \text{ nm}$. For comparison, the resistivity of CVD-W nucleation layer with the thickness of $\sim 18 \text{ nm}$ was $\sim 25 \mu\Omega \text{ cm}$.⁶ Interestingly, as the film thicknesses decreased, the resistivities of ALD-W (A) and ALD-W (B) films prepared from SiH_4 reduction of WF_6 significantly increased but the increase in the resistivity of ALD-W film (C) film prepared from B_2H_6 reduction increased only slightly. Thus, B_2H_6 -based ALD-W film has an advantage from the point of view of continuous thickness scaling of nucleation layer. Relatively higher film resistivities of ALD-W films can be explained by considering impurity incorporation, film phase, crystallinity, and grain size, which are further discussed later.

The composition and impurities of ALD-W films were analyzed using XPS depth profiling (Fig. 3). It is noteworthy that the results of the XPS analysis do not show that any impurities such as O and F were detected in ALD-W films irrespective of deposition processes. Approximately 5–6 atom % of Si impurity was detected in

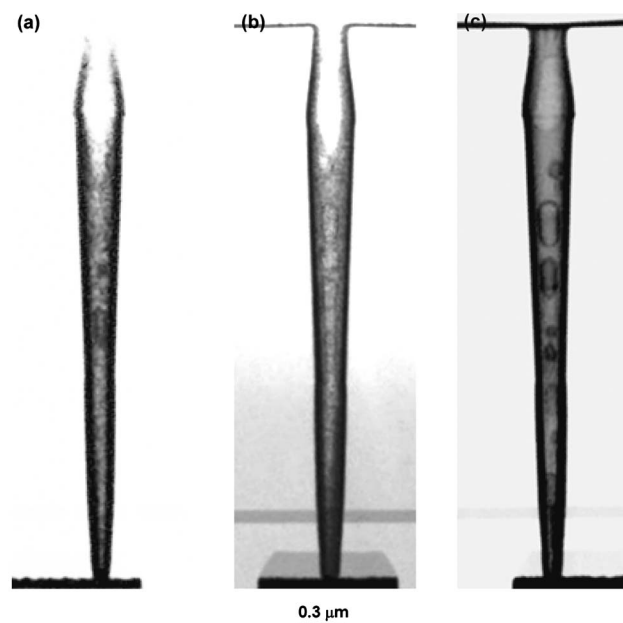


Figure 1. The step coverages of ALD-W films at UHAR contact (AR ~ 15): (a) ALD-W (A), (b) ALD-W (B), and (c) ALD-W (C). 5 nm thick TiCl_4 -based CVD-TiN as a barrier layer was deposited prior to ALD-W deposition.

SiH_4 -based ALD-W films (Fig. 3a and b). It is thought that Si from the decomposition of SiH_4 at the SiH_4 pulsing step is incorporated in SiH_4 -based ALD-W films. Herner et al.¹² reported that a monolayer Si was formed by SiH_4 pretreatment at $\sim 410^\circ\text{C}$ used in CVD-W plug process. So, a successive SiH_4 pulsing step in ALD could be the reason for Si incorporation. For comparison, the results of CVD-W nucleation layer deposited using WF_6 and SiH_4 showed no Si impurities.⁶ The XPS depth profile of B_2H_6 -based ALD-W film (Fig. 3c) showed a B content of $\sim 5 \text{ atom\%}$, which indicates that a small amount of B_2H_6 was thermally decomposed at 300°C ¹¹ and incorporated into the film. Thus, the Si and B impurities can be one of the reasons for the increase of the resistivities of ALD-W films investigated in this study by impurity scattering.^{6,13} Although no F was detected in XPS analysis, in order to more sensitively detect F impurities SIMS depth profiling was performed (Fig. 4). F concentration was much lower in B_2H_6 -based ALD-W film ($\sim 1.2 \times 10^{17}/\text{cm}^3$) as compared to those of SiH_4 -based ALD-W films ($1 \sim 5.4 \times 10^{20}/\text{cm}^3$). This indicates that B_2H_6 pulsing is more effective in reducing WF_x absorbed on the surface and making pure metal W film. The CVD-W film deposited using WF_6 and SiH_4 also

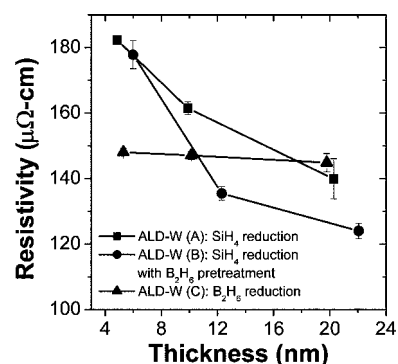


Figure 2. The resistivities of ALD-W films as function of film thicknesses.

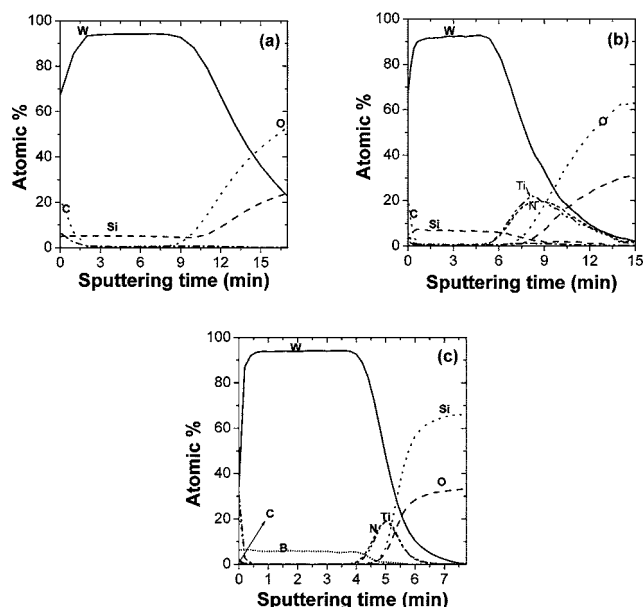


Figure 3. XPS depth profiles of ALD-W films.

showed F content of $\sim 3.5 \times 10^{20}/\text{cm}^3$ (not shown here) and this indicates that F content in ALD-W films of this study is not a major factor in the increase of their resistivities.

Figure 5 shows the glancing angle XRD patterns of ALD-W films. The XRD patterns of both SiH_4 -based ALD-W films show peaks from A15 primitive cubic β -W¹⁴⁻¹⁶ or β -W (200) [$2\theta = 35.56^\circ$] and (211) [$2\theta = 43.96^\circ$] apart from the peaks from A2 body-centered-cubic (bcc) α -W. This indicates that the films are mixtures of α -W and β -W. Comparing the XRD peaks of ALD-W (A) and ALD-W (B), we found that the B_2H_6 pretreatment caused β -W phase to form more favorably. β -W is known as a metastable phase and is reported to have significantly higher resistivity of as high as $100\text{--}300 \mu\Omega \text{ cm}^{16}$ than the bulk resistivity of thermodynamically stable α -W ($5.6 \mu\Omega \text{ cm}$). Thus, the formation of high-resistivity β -W phase in SiH_4 -based ALD-W films can be one of the main reasons for the increase of the film resistivity, which is clearly different from the results of CVD-W nucleation layer deposited from WF_6 and SiH_4 showing the formation of α -W single phase.⁶ Interestingly, the XRD result of B_2H_6 -based ALD-W film [ALD-W (C)]

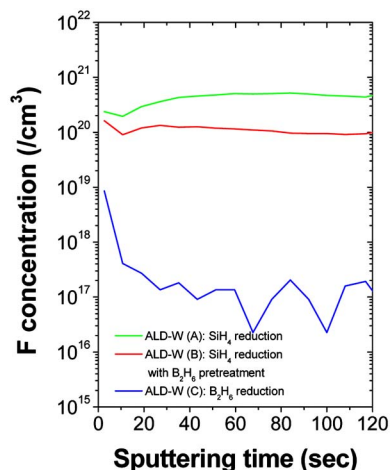


Figure 4. SIMS depth profile of ALD-W films showing the content of F impurity.

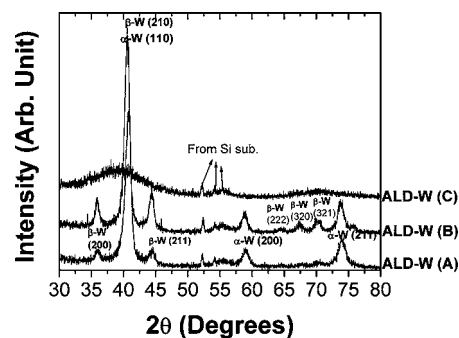


Figure 5. Glancing angle XRD spectra of ALD-W films. The incidence angle of X-ray was $\sim 1^\circ$.

showed no specific peak, indicating that the film was amorphous or an amorphous-like structure, which is known to cause the film resistivity to increase.

To further determine the phase and microstructure, the films were analyzed using TEM. The plan-view TEM bright-field (BF) images of 20 nm thick ALD-W (A) film (Fig. 6a) showed that the film formed a polycrystalline structure with the grain size ranging from $\sim 9\text{--}17$ nm and not an amorphous one. Indexing of selected area diffraction pattern (SADP) showed a clear ring pattern of bcc α -W. Diffraction rings, which can be indexed as β -W (200) ($d = 2.52 \text{ \AA}$) and β -W (211) ($d = 2.08 \text{ \AA}$), respectively, were observed close to α -W (110) ($d = 2.238 \text{ \AA}$). The XTEM image of ALD-W (A) (Fig. 6b) showed a crystalline microstructure with a relatively rough film surface. The TEM analysis of ALD-W (B) showed a very similar plan-view image (Fig. 7a) to that of ALD-W (A). The sharp diffraction pattern from β -W phase matches well with the XRD results. However, the grain size slightly increased to $\sim 11\text{--}21$ nm. Slightly larger grains of ALD-W (B) than those of ALD-W (A) partly explain its relatively lower resistivity (see Fig. 2). Another reason why the ALD-W (B) showed a lower resistivity in spite of having the relatively larger amount of β -W phase compared with ALD-W (A) is its lower roughness. The root-mean-square (rms) roughness at ~ 20 nm thickness was ~ 1 nm for ALD-W (B) and ~ 2 nm for ALD-W (A), respectively. The XTEM image of ALD-W (B) (Fig. 7b) showed the relatively lower surface roughness as compared to ALD-W (A).

Figure 8a shows the plan-view TEM BF images of 20 nm thick B_2H_6 -based ALD-W film [ALD-W (C)]. Compared to Fig. 6a and 7a, a plan-view TEM image seems to be featureless, indicating that the film forms the amorphous structure. This was confirmed by the corresponding faint SADP. Thus, in TEM analysis, the amorphous nature of B_2H_6 -based ALD-W film has a clear advantage in terms of barrier performance to WF_6 diffusion occurring at the subsequent plug-fill step compared to SiH_4 -based ALD-W films. The XTEM

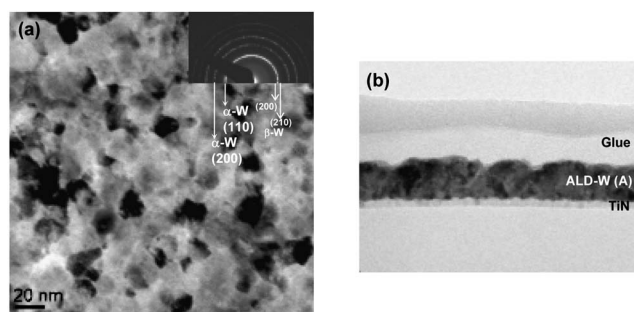


Figure 6. (a) Plan-view TEM BF image and (b) cross-sectional view TEM BF image of ALD-W (A) deposited on TiCl_4 -based CVD-TiN. The inset in (a) shows the selected area electron diffraction pattern.

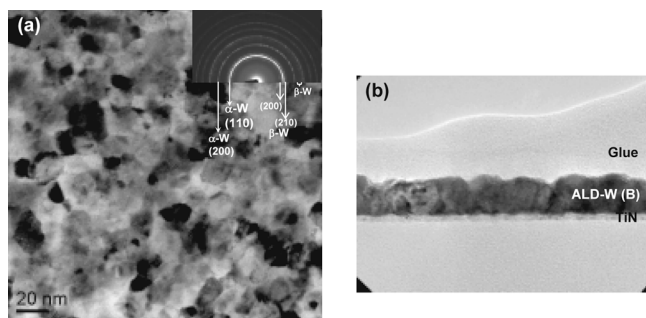


Figure 7. (a) Plan-view TEM BF image and (b) cross-sectional view TEM BF image of ALD-W (B) deposited on TiCl_4 -based CVD-TiN. The inset in (a) shows the selected area electron diffraction pattern.

image of 20 nm thick ALD-W (C) film (Fig. 8b) showed very smooth surface topography as compared to those of ALD-W (A) and ALD-W (B).

The thermal stability and phase transformation behavior of ALD-W films were investigated because their potential applications include the electrode for gate or capacitor in semiconductor device or diffusion barrier for Cu metallization. Figure 9a shows the change in sheet resistances of ALD-W/TiN/SiO₂ stacks as a function of annealing temperature. In the case of ALD-W (A) and ALD-W (B), when the annealing temperature increased to 800°C, the sheet resistance decreased significantly. XRD analysis with annealing temperature (Fig. 9b and c) showed that the peak intensity from α -W (110) nearby $2\theta = 40^\circ$ increased and the full width at half maximum (fwhm) became narrower after annealing at 800°C. This indicated that the grain size slightly increased after annealing, resulting in the decrease in their sheet resistances. XRD analysis also showed that the peaks from β -W phase disappeared after annealing at 800°C. As the annealing temperature increased to 900°C, the peak intensities from α -W increased, which matches well with the sheet resistance change shown in Fig. 9a. Thus, the significant decrease in sheet resistance of ALD-W (A) and ALD-W (B) after annealing at 800 and 900°C is mainly due to the phase transformation from β -W with high resistivity to α -W with low resistivity, not the increase in the grain size. However, the remarkable change in sheet resistance of the ALD-W(C)/TiN/SiO₂ stack was not observed when annealing continued to 900°C. This indicates that the structural change of ALD-W (C) film that includes an amorphous phase is negligible. In fact, XRD analysis (Fig. 9d) confirms that ALD-W (C) film kept its amorphous state until annealing at 900°C.

Effect of ALD-W nucleation layers on the properties of CVD-W films.—The traditional CVD W-plug process is composed of two steps:⁴ W nucleation and W-plug fill. Prior to W nucleation, TiN is

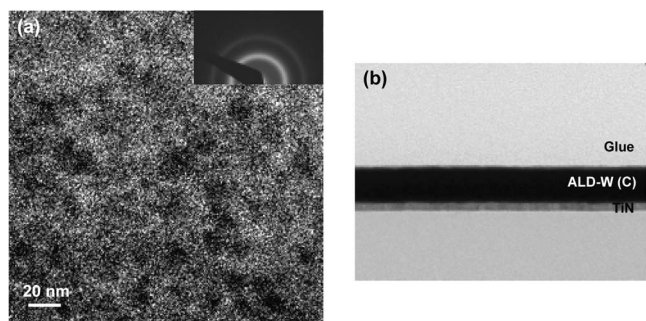


Figure 8. (a) Plan-view TEM BF image and (b) cross-sectional view TEM BF image of ALD-W (C) deposited on TiCl_4 -based CVD-TiN. The inset in (a) shows the selected area electron diffraction pattern.

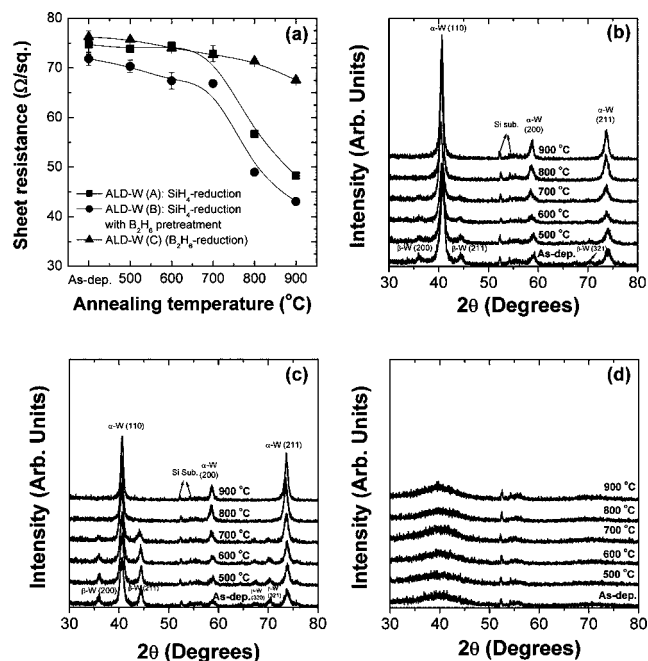


Figure 9. (a) Sheet resistance change of ALD-W/TiN/SiO₂ film stacks, (b) XRD analysis of ALD-W(A)/TiN/SiO₂ film stack, (c) ALD-W(B)/TiN/SiO₂ film stack, and (d) ALD-W(C)/TiN/SiO₂ film stack as a function of annealing temperature.

typically deposited as a barrier layer. Thus, the total W-plug stack is generally composed of plug-fill CVD-W/W nucleation layer/TiN. As it is well known that the underlayer film has some effect on the properties of the film growing on it in the many thin film systems,¹⁷⁻¹⁹ it is necessary to understand how the ALD-W underlayers affect the growing CVD-W films on them. In this study, 5 nm thick TiCl_4 -based CVD-TiN film was used as the barrier layer and a plug-fill CVD-W film was deposited at $\sim 390^\circ\text{C}$ using H_2 reduction of WF_6 .

Figure 10 shows the resistivities of total W-plug stacks of CVD-W/ALD-W/CVD-TiN. Their resistivities are very important because they can directly affect the contact resistance obtained by W-plug process. Here, as the resistivities of CVD-TiN and ALD-W films are much higher ($\sim 600 \mu\Omega \text{ cm}$ for CVD-TiN and $125\text{--}150 \mu\Omega \text{ cm}$ for

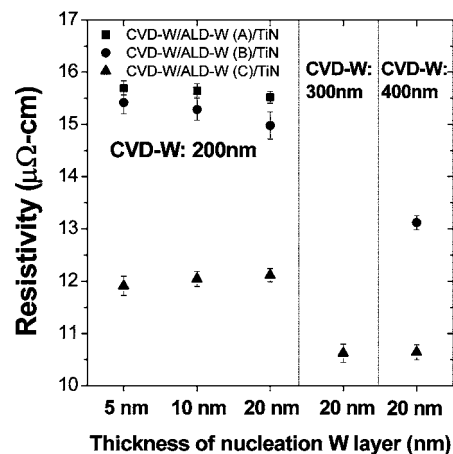


Figure 10. The resistivity of film stack of CVD-W/ALD-W/CVD-TiN with the thickness of ALD-W film and CVD-W film. TiN film 5 nm thick was deposited using the reaction of TiCl_4 and NH_3 at 580°C and CVD-W was prepared using H_2 reduction of WF_6 at $\sim 390^\circ\text{C}$.

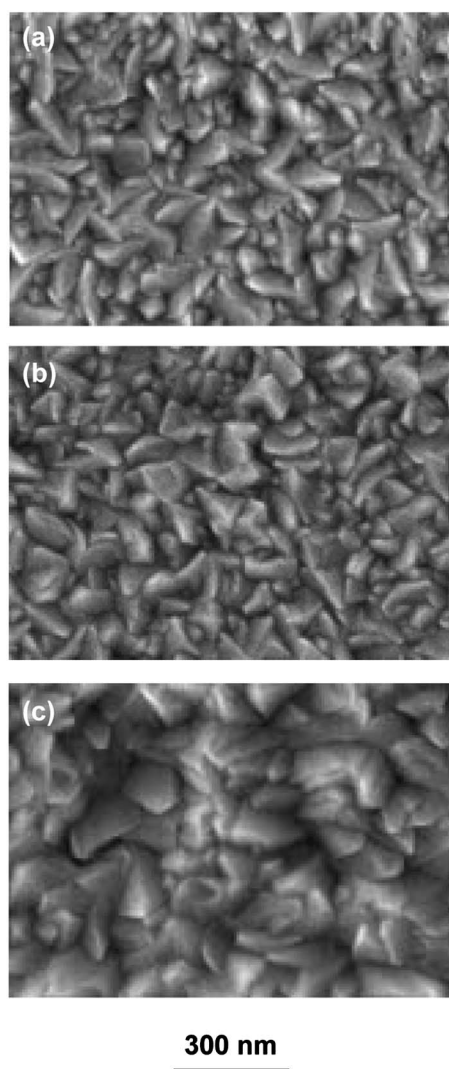


Figure 11. Plan-view SEM images of CVD-W films (200 nm) deposited on (a) ALD-W (A), (b) ALD-W (B), and (c) ALD-W (C). The thickness of ALD-W film is 20 nm.

ALD-W films) and the thicknesses are much thinner (5 nm for CVD-TiN and 5–20 nm for ALD-W films) than those of CVD-W film, the resistivity of the total film stack is dominantly determined by that from CVD-W film. Interestingly, the film stack of CVD-W/ B_2H_6 -based ALD-W [ALD-W (C)]/CVD-TiN showed a much lower resistivity compared to those with SiH_4 -based ALD-W films [ALD-W (A) and ALD-W (B)], irrespective of the thickness of the nucleation layer. Figure 10 also shows that the resistivities of film stacks decrease with increasing CVD-W film thickness. However, when the CVD-W film thickness exceeded 300 nm, the resistivity of film stack was not further decreased. As mentioned earlier, as it is the resistivity of CVD-W film that determines the resistivity of total film stack, it is important to understand why the resistivity of CVD-W film is different with W nucleation process.

Here, when we compare the resistivity of the film with the same thickness, the thickness effect^{6,13,20} can be ignored. As the deposition conditions for CVD-W film are the same, the impurities incorporation such as F and O can also be ignored when comparing resistivity. In fact, we were able to confirm through the AES analysis (not shown here) that there was no difference in the impurities content such as F and O of CVD-W films deposited on different ALD-W films. The AFM analysis also indicated that a lower resistivity of film stack with B_2H_6 -based ALD-W film is not related with the

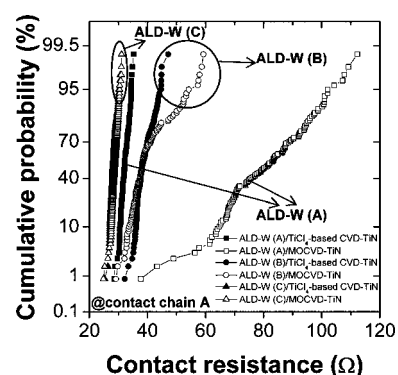


Figure 12. The distribution of contact resistances with ALD-W films at the contact chains A connecting Al metal line with W bit line. Here, the aspect ratio of contact chain A was ~ 15 . As a barrier layer, $TiCl_4$ -based CVD-TiN film (closed symbol) or MOCVD-TiN film (open symbol) were used.

roughness.^{6,13,20} In fact, the rms roughness of CVD-W films deposited on both SiH_4 -based ALD-W nucleation layers was much smaller (10–12 nm) than one on B_2H_6 -based ALD-W nucleation layer (~ 20 nm) when the thickness of plug-fill CVD-W was 200 nm. Thus, much lower resistivity of film stack with B_2H_6 -based ALD-W film suggests that the microstructure characterized by the grain size is the dominant factor that determines the film resistivity. Figure 11 shows the plan-view SEM images of CVD-W films (200 nm) deposited on different ALD-W films. It clearly showed that CVD-W film deposited on ALD-W (C) has much larger-sized grains than the ones deposited on both ALD-W (A) and ALD-W (B), which contributes to the lower resistivity of the film stack with ALD-W (C) as a nucleation layer.

Comparison of electrical performances of ALD-W films as nucleation layers for W-plug process of DRAM.—In this section, the contact resistances of integration schemes with ALD-W films as nucleation layers for W-plug process were comparatively investigated at 70 nm design-rule DRAM. Here, W-plug process was used at the contact connecting the metal line and W bit line of DRAM with the stacked capacitor. Figure 12 shows the contact resistance distribution with different deposition processes of barrier and nucleation layers at the contact chains structure with the aspect ratio of ~ 15 (contact chain A). When the $TiCl_4$ -based CVD-TiN film was used as barrier layer, we could obtain stable contact resistances for all the integration schemes at such UHAR contact but the contact resistances were different with nucleation processes. Figure 12

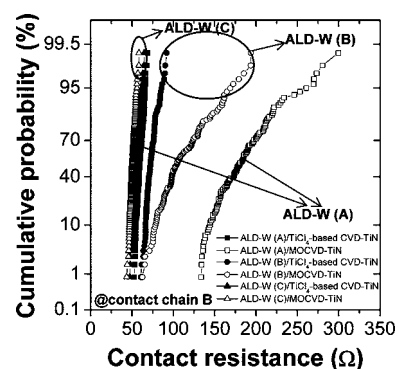


Figure 13. The distribution of contact resistances with ALD-W films at the contact chains B connecting Al metal line with W bit line. Here, the aspect ratio of contact chain A was ~ 17 . As a barrier layer, $TiCl_4$ -based CVD-TiN film (closed symbol) or MOCVD-TiN film (open symbol) were used.

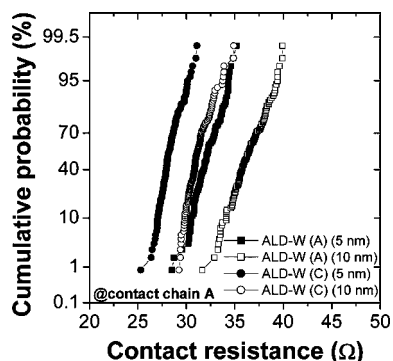


Figure 14. The distribution of contact resistances with different thicknesses of ALD-W films at the contact chains A (AR \sim 15) connecting Al metal line with W bit line. As a barrier layer, TiCl₄-based CVD-TiN film (closed symbol) was used.

clearly shows that the integration scheme with ALD-W (C) as a W nucleation layer shows a much lower contact resistance than those with ALD-W (A) or ALD-W (B). This is due to the much lower resistivity of the total film stack consisting of W-plug, as shown by Fig. 10, rather than the difference in the plug-filling capability.

Interestingly, when the MOCVD-TiN film was used as a barrier layer, the integration scheme with ALD-W (A) showed higher contact resistance and its distribution at 200 mm wafer became poor. It is thought that the step coverage of the barrier layer, TiN, was degraded with MOCVD as compared to TiCl₄-based CVD. This is possibly due to the fact that generally, the deposition for MOCVD-TiN is performed in the diffusion-controlled regime to obtain high-quality film. That the precursor is too bulky for MOCVD to transport into the bottom of UHAR contact could be another reason for poor step coverage. When the step coverage of TiN is not sufficient at UHAR contact, the growth of ALD-W film is more likely to occur on the interlayer dielectric material, SiO₂, and not TiN, especially at the bottom of the contact. Meanwhile, it is known that nucleation and growth of ALD-W film deposited using alternating exposures of WF₆ and SiH₄ or Si₂H₆ on SiO₂ is difficult^{11,21} and this causes the degradation in step coverage of W nucleation layer even though W is deposited by ALD. The degradation in the step coverage of the nucleation layer again degrades W-plug filling, resulting in the increase in contact resistance. It was recently reported that the B₂H₆ pretreatment enhanced the nucleation and growth of ALD-W film on SiO₂ surface.¹¹ This could enhance the step coverage of ALD-W nucleation layer deposited by SiH₄ reduction of WF₆ even though the step coverage of the underlayer, TiN, was not satisfactory. In this study, the contact resistance with ALD-W (B) nucleation layer kept lower values, except for some positions of the wafer when the MOCVD-TiN was used. This suggests that B₂H₆ pretreatment provides some flexibility in terms of choosing the method for depositing TiN underlayer for W-plug process. In terms of W nucleation on SiO₂, B₂H₆ reduction of WF₆ could provide the most effective passway and this assured stable and low contact resistance even when the MOCVD-TiN was used as the barrier layer.

Figure 13 shows the contact resistance distribution when the aspect ratio was further increased to \sim 17 [contact chain B]. All the integration schemes show stable and low contact resistances with TiCl₄-based CVD-TiN, which is similar to Fig. 12. Even though B₂H₆ pretreatment was done prior to ALD-W deposition [ALD-W (B)], the distribution of contact resistance was degraded with MOCVD-TiN barrier layer and its values were higher at all the positions of 200 mm wafer than those with TiCl₄-based CVD-TiN. The contact resistance of the integration scheme with ALD-W (A) further increased and its distribution worsened with MOCVD-TiN. However, with ALD-W (C) deposited by B₂H₆ reduction, we could obtain a stable contact resistance irrespective of the deposition pro-

cess for barrier layer (see Fig. 12 and 13) and its contact resistance was significantly lower as compared with the integration schemes with ALD-W film deposited by SiH₄ reduction.

Figure 14 shows the effect of ALD-W film thickness on the contact resistance. Here, TiCl₄-based CVD-TiN was used as a barrier layer. From Fig. 14, it is clear that the contact resistance decreased as the thicknesses of ALD-W films decreased. This is due to the decrease in cross-sectional area occupied by ALD-W film with a higher resistivity (Fig. 2) and the increase of cross-sectional area occupied by low-resistivity plug-fill CVD-W film (Fig. 10). The minimum thickness of the nucleation layer evaluated as a nucleation layer in this study was as thin as \sim 5 nm and the successful integration of this ultrathin nucleation layer indicates that ALD provides uniform nucleation and accurate thickness control.

Conclusions

In summary a thin and conformal W nucleation layer is essential for successfully filling the UHAR small plug as the device is ever-shrinking. In this study, the properties of three kinds of ALD-W films (two SiH₄-based ALD-W films and one B₂H₆-based ALD-W film) were comparatively characterized and investigated as nucleation layers for W-plug process of 70 nm design-rule DRAM. Though all the ALD-W films had excellent step coverage irrespective of deposition processes, their resistivities were high, ranging between \sim 125 and \sim 180 $\mu\Omega$ cm with film thickness. High resistivities of SiH₄-based ALD-W films are mainly due to the Si incorporation in the film and the formation of metastable β -W phase with high resistivity. The high resistivity of B₂H₆-based ALD-W film is due to the B incorporation and the formation of amorphous phase. The formation of amorphous W film as a nucleation layer for W-plug process has many advantages such as superior diffusion barrier properties, less-sensitive thickness effect of film resistivity, and the large-size grains formation growing on it, leading to lowering the resistivity of the W-plug stack. The results demonstrated that the integration scheme with B₂H₆-based ALD-W film showed a much lower contact resistance at UHAR contact. The B₂H₆-based process also has advantages in terms of nucleation on SiO₂. The enhanced nucleation on SiO₂ by B₂H₆-based process provides a stable and low contact resistance with MOCVD-TiN as the barrier layer with limited step coverage. By the same argument, the B₂H₆ pretreatment prior to ALD-W formation using SiH₄ reduction contributed to the enhancement of the nucleation and assured stable and low contact resistance at the UHAR contact in this study.

Hynix Semiconductor, Inc., assisted in meeting the publication costs of this article.

References

- H. Kim, *J. Vac. Sci. Technol. B*, **21**, 2231 (2003).
- M. Leskelä and M. Ritala, *Thin Solid Films*, **409**, 138 (2002).
- <http://www.itrs.net/Links/2005ITRS/Interconnect2005.pdf>
- J. E. J. Schmitz, *Chemical Vapor Deposition of Tungsten and Tungsten Silicides*, Noyes Publications, Park Ridge, NJ (1991).
- T. Omstead, G. C. D' Couto, S.-H. Lee, P. Wongsenkaum, J. Collins, and K. Levy, *Solid State Technol.*, **51**, 45 (2002).
- S.-H. Kim, E.-S. Hwang, S.-H. Pyi, H.-J. Sun, J.-W. Lee, J.-K. Kim, N. Kaw, H. Sohn, and J. Kim, *J. Electrochem. Soc.*, **152**, C408 (2005).
- J. W. Klaus, S. J. Ferro, and S. M. George, *Thin Solid Films*, **360**, 145 (2000).
- M. Yang, H. Chung, A. Yoon, H. Fang, A. Zhang, C. Knepler, R. Jackson, J. S. Byun, A. Mak, M. Eizenberg, M. Xi, M. Kori, and A. K. Sinha, in *Conference Proceedings ULSI XVII*, p. 655, MRS, Warrendale, PA (2002).
- S.-H. Lee, L. Gonzalez, Josh Collins, K. Ashitani, and K. Levy, in *Conference Proceedings ULSI XVII*, p. 649, MRS, Warrendale, PA (2002).
- Y. Mizoguchi, K. Suzuki, M. Tachibana, and D. Abe, in *Conference Proceedings ULSI XVIII*, p. 451, MRS, Warrendale, PA (2003).
- S.-H. Kim, E.-S. Hwang, B.-M. Kim, J.-W. Lee, H.-J. Sun, T. E. Hong, J.-K. Kim, H. Sohn, J. Kim, and T.-S. Yoon, *Electrochem. Solid-State Lett.*, **8**, C155 (2005).
- S. B. Herner, S. A. Desai, A. Nak, and S. G. Ghanayem, *Electrochem. Solid-State Lett.*, **2**, 398 (1999).
- S. M. Rossnagel, *J. Vac. Sci. Technol. B*, **20**, 2328 (2002).
- A. K. Sinha, *Prog. Mater. Sci.*, **15**, 92 (1972).
- Y. G. Shen, Y. W. Mai, Q. C. Zhang, D. R. McKenzie, W. D. McFall, and W. E. McBride, *J. Appl. Phys.*, **87**, 117 (2000).
- P. M. Petroff, A. K. Sinha, T. T. Sheng, H. J. Levinstein, and F. B. Alexander, *J.*

- Appl. Phys.*, **44**, 2545 (1973).
17. J. M. E. Harper and K. P. Rodbell, *J. Vac. Sci. Technol. B*, **15**, 763 (1997).
18. J.-M. Yang, I. S. Choi, Y. S. Kim, J.-C. Park, S.-M. Lee, T.-E. Hong, Y.-B. Park, S.-Y. Lee, and I. W. Kim, *J. Appl. Phys.*, **91**, 9788 (2002).
19. J.-W. Lee, J. K. Kim, S.-H. Kim, H.-J. Sun, H.-S. Yang, H. C. Sohn, and J. W. Kim, *J. Appl. Phys.*, **43**, 8008 (2004).
20. T. S. Kuan, C. K. Inoki, G. S. Oehrlein, K. Ross, Y.-P. Zhao, G.-C. Wang, S. M. Rossnagel, and C. Cabral, *Mater. Res. Soc. Symp. Proc.*, **612**, D7.1.1 (2000).
21. J. W. Elam, C. E. Nelson, R. K. Grubbs, and S. M. George, *Thin Solid Films*, **386**, 41 (2001).